Applied Biochemistry and Biotechnology (2025) 197:910–925
https://doi.org/10.1007/s12010-024-05068-1

ORIGINAL ARTICLE

A Self-Powered Enzymatic Glucose Sensor Utilizing Bimetallic Nanoparticle Composites Modified Pencil Graphite Electrodes as Cathode

Gamze Emir[1] · Yusuf Dilgin[1] · Samet Şahin[2,3] · Cahit Akgul[1]

Accepted: 19 September 2024 / Published online: 27 September 2024

Abstract

Enzymatic biofuel cells (EBFC) are promising sources of green energy owing to the benefits of using renewable biofuels, eco-friendly biocatalysts, and moderate operating conditions. In this study, a simple and effective EBFC was presented using an enzymatic composite material-based anode and a nonenzymatic bimetallic nanoparticle-based cathode respectively. The anode was constructed from a glassy carbon electrode (GCE) modified with a multi-walled carbon nanotube (MWCNT) and ferrocene (Fc) as a conductive layer coupled with the enzyme glucose oxidase (GOx) as a sensitive detection layer for glucose. A chitosan layer was also applied to the electrode as a protective layer to complete the composite anode. Chronoamperometry (CA) results show that the MWCNT-Fc-GOx/GCE electrode has a linear relationship between current and glucose concentration, which varied from 1 to 10 mM. The LOD and LOQ were calculated for anode as 0.26 mM and 0.87 mM glucose, respectively. Also the sensitivity of the proposed sensor was calculated as 25.71 μ A/mM. Moreover, the studies of some potential interferants show that there is no significant interference for anode in the determination of glucose except ascorbic acid (AA), uric acid (UA), and dopamine (DA). On the other hand, the cathode consisted of a disposable pencil graphite electrode (PGE) modified with platinum-palladium bimetallic nanoparticles (Nps) which exhibit excellent conductivity and electron transfer rate for the oxygen reduction reaction (ORR). The constructed EBFC was optimized and characterized using various electroanalytical techniques. The EBFC consisting of MWCNT-Fc-GOx/GCE anode and Pt-PdNps/PGE cathode exhibits an open circuit potential of 285.0 mV and a maximum power density of 32.25 μW cm^{-2} under optimized conditions. The results show that the proposed EBFC consisting of an enzymatic composite-based anode and bimetallic nanozyme-based cathode is a unique design and a promising candidate for detecting glucose while harvesting power from glucose-containing natural or artificial fluids.

Extended author information available on the last page of the article

Graphical Abstract

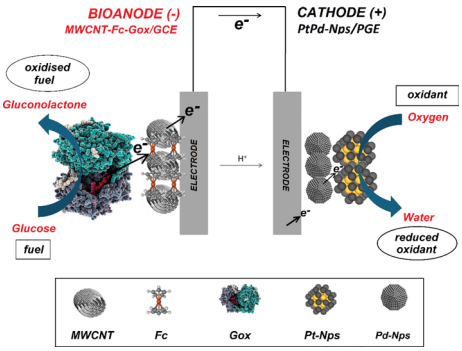

Keywords Enzymatic biofuel cell (EBFC) · Glucose oxidase (GOx) · Nanozyme · Self-powered glucose sensor (SPGS) · Ferrocene (Fc) · Bimetallic nanoparticles

Introduction

Biofuel cells (BFCs) are electrochemical devices that generate electrical energy using organic molecules produced during metabolic processes as a fuel and a renewable biological catalyst. They are considered environmentally friendly and sustainable energy options [1–5]. Two main BFCs have become prominent: enzymatic biofuel cells (EBFCs) that use purified oxidoreductase enzymes and microbial biofuel cells (MBFCs) that use microorganisms [3–6]. EBFCs are attractive devices that directly convert the chemical energy stored in the fuel into electricity using enzymes as biocatalysts. These types of fuel cells are commonly employed in biosensors and bioelectronic devices. EBFCs transform enzymatic chemical reactivity into electrical power output by oxidizing fuel at the anode and reducing an oxidant at the cathode [4–6]. EFBCs are known as renewable and environmentally friendly technologies due to their remarkable properties such as easy miniaturization, portability, working conditions around room temperatures, and physiological pH. Furthermore, EBFCs offer advantages such as high conversion efficiency and versatility as they can generate electrical energy from various organic substrates [5–7]. Separating the anodic and cathodic parts is unnecessary due to the high selectivity of enzymes. This enables the development of miniature and membraneless EBFCs implanted in the human body to potentially power medical devices [5, 8–10]. However, current approaches face several challenges, such as the need for specific pH and temperature conditions, difficulties in stabilizing enzymes to the electrode surfaces, and inadequacies in electron transfer rate between the electrodes [9].

Numerous techniques have been developed to improve the enzyme immobilization, power output, and stability of EBFCs. Various enzyme immobilization techniques, including direct immobilization, cross-linking with bifunctional linker molecules, and self-assembled monolayers, have already been applied to EBFCs [10, 11]. Various electrode surface modifications were also performed using novel materials to promote electron transfer between the redox enzyme and the electrode [10–13]. For this reason, enzymatic electrodes have been prepared using a variety of materials, like gold nanoparticles [14–16],

carbon nanotubes, redox polymers, metal complexes [17, 18], or electron transfer mediators, which include osmium (Os), benzoquinone, polyvinyl ferrocene, ferrocene (Fc), and its derivatives [19, 20]. Redox mediators are chemicals with electrochemical activity and widely used in biosensors and biofuel cells. Ferrocene (Fc) and its derivatives are notable among all the mediators due to their nontoxicity to the human body and solubility in various solvents, including water and ethanol [3, 20]. Carbon nanotubes (CNTs) have also been used to improve the properties of Fc-modified electrodes because of their unique biocompatibility properties and excellent electrical conductivity [3, 17, 20].

Improving the oxygen reduction reaction (ORR) activity is essential for fuel cell development [21]. The glucose/O_2 biofuel cell, with a glucose oxidizing anode and an O_2-reducing cathode, could become an in vivo electricity source to power integrated medical devices. Recent developments in nanotechnology have led to the designing of new artificial enzymes called nanozymes. Nanozymes have numerous advantages including diverse enzyme-mimicking activities, low cost, high stability, robustness, unique surface chemistry, ease of surface tunability, and biocompatibility. These advantages have allowed their integration into a wide range of biosensing applications [22, 23]. Several biosensing systems have been developed using metal, metal oxide, and metal–organic framework-based nanozymes [22–25].

In this work, we designed a simple EBFC configuration operating in ambient and physiological conditions containing enzymatic composite material-based anode and nonenzymatic bimetallic nanoparticle-based cathode. Glucose was selected as the substrate due to its suitability as a biological fuel and its prevalence in various biological fluids including blood, tears, saliva, and sweat. In our system, glucose is oxidized by glucose oxidase (GOx) at the anode and oxygen is reduced by bimetallic nanoparticle composite material at the cathode. The anode consists of a GOx immobilized on a glassy carbon electrode (GCE) modified with an MWCNT and Fc. On the other hand, the cathode consisted of a pencil graphite electrode modified with platinum (Pt) and palladium (Pd) metal nanoparticles (MNps). Pencil graphite electrode (PGE) was preferred as an electrode material at the cathode because of its advantages, such as electrochemical activity, commercial accessibility, good mechanical strength, disposability, low cost, and simple modification procedure [23, 26]. This novel design of EBFC has produced significant electrical power that can be used for various applications, including glucose detection or powering medical devices.

Materials and Methods

Reagents

Analytical-grade chemicals were used without further purification. GOx (from *Aspergillus niger* type 77 units/mg) was purchased from Sigma-Aldrich. Stock solutions of GOx were prepared using 0.1 M phosphate buffer solution (PBS) with pH 7.0, and stored at − 20 °C until used. Multi-walled carbon nanotubes, ferrocene, palladium (II) chloride ($PdCl_2$), and chloroplatinic acid (H_2PtCl_6) solution 8% wt. in H_2O were supplied from Sigma-Aldrich.

Chemicals such as potassium phosphate dibasic ($Na_2HPO_4.2H_2O$), potassium phosphate monobasic ($NaH_2PO_4.2H_2O$), potassium chloride (KCl), sodium hydroxide (NaOH), chitosan (medium molecular weight), and D-(+)-glucose (≥ 99.5%) were purchased from Merck. Potassium ferricyanide ($K_3[Fe(CN)_6]0.3H_2O$) and potassium ferrocyanide ($K_4[Fe(CN)_6]0.3H_2O$) were purchased from Sigma-Aldrich. All solutions were prepared

with ultrapure water using the Elga Option Q7B water purification system (18.2 μW cm^{-1}). 0.10 M KCl containing 0.1 M PBS with pH 7.0 was used as an electrolyte to characterize electrodes and biofuel cells.

Apparatus and Electrochemical Measurements

All electrochemical measurements including electrochemical impedance spectroscopy (EIS), cyclic voltammetry (CV), linear sweep voltammetry (LSV), amperometry, and open circuit potential (OCP) tests were run using a Metrohm model Autolab PGSTAT 128N Potentiostat/Galvanostat. Before carrying out the electrochemical tests and between each successive addition of glucose, it was ensured that the solutions were purged with either air or argon. The stock glucose solutions were allowed to mutarotate for at least 24 h before use and then stored in a refrigerator at 4 °C. CV and amperometric techniques were employed to characterize the electrodes. In these studies, a three-electrode cell consisting of an unmodified or modified working, an Ag/AgCl (KCl, 3 M) reference electrode, and a platinum wire auxiliary electrode was used.

Fabrication of the Electrodes

Preparation of Anode Electrodes (MWCNT-Fc-GOx/GCE)

Before a modification step, GCEs were polished with different grain sizes (1 µm, 0.3 µm, and 0.05 µm, respectively) alumina on a polishing cloth. Then, GCE was sonicated in ethanol and ultrapure water and dried with an IR lamp. Then, the dried electrodes were placed in an electrochemical cell, and a preconditioning step of 20 scans at 50 mVs^{-1} between − 0.4 and 0.4 V (vs. Ag/Ag^{+}) was applied in 0.1 M KCl with the CV method. After the preconditioning step, the electrodes were washed with de-ionized water and dried in front of IR lamb for 5 min. After the cleaning procedure of GCE, 25 mM Fc containing 20 mg/mL MWCNT solution was prepared and sonicated for 15 min in an ultrasonic bath. Then, 10.0 µL from that solution was added onto the GCE surface and dried with IR lamb for 5 min in every 1.0 µL addition. Twenty milligrams per milliliter GOx mixed in 0.10 M PBS with pH 7.0 was then dropped on the surface of MWCNT-Fc-GCE, and dried for 2 h at the room temperature. The preparation of the enzyme electrode is finalized by the addition of the % 0.5 chitosan solution in acetic acid. The enzyme electrodes were stored at + 4 °C when not in use.

Preparation of Cathode Electrodes (PtNps/PGE, PdNps/PGE, and Pt-PdNps/PGE)

Platinum nanoparticles (PtNps) have been efficiently deposited onto the surface of PGE using an electrochemical method. It was achieved by recording cyclic voltammograms in a 5.0 mM solution of H_2PtCl_6 containing 0.10 M KCl from 0.8 to − 0.8 V at a scan rate of 50 mVs^{-1} for 30 cycles (Fig. S5A). Electrodeposition mechanism of $PtCl_6^{2-}$ was reported by our previous study [26]. Palladium nanoparticles (PdNps) were also efficiently deposited onto the surface of PGE using an electrochemical method [27]. Cyclic voltammograms were recorded in a supporting electrolyte of 0.10 M KCl and 5.0 mM $PdCl_2$ at a scan rate of 25 mVs^{-1} for 30 cycles within a potential range of 0.40 V to − 0.25 V (Fig. S5B). For the PtPd-Nps electrodes, 5.0 mM of H_2PtCl_6 and 5.0 mM of $PdCl_2$ containing 0.1 M KCl

solutions were used. This is also achieved by recording CV under the same conditions as PtNps and PdNps deposition, respectively (Fig. S5C).

Characterization of Electrodes

SEM and EDX images of both unmodified and modified PGE electrodes were taken to provide an accurate analysis of the surface changes resulting from the electrochemical processes. Scanning electron microscopy (SEM–EDX) images were taken at COBILTUM (Science and Technology Application and Research Center) of the Çanakkale Onsekiz Mart University with a device of JEOL JSM-7100-F. The electrodes were electrochemically characterized using CV and EIS techniques which were recorded in a solution containing 5.0 mM $Fe(CN)_6^{3-/4-}$ + 0.10 M KCl.

Fuel Cell Tests and Real Sample Analysis

The biofuel cells were characterized by recording LSV using MWCNT-Fc-GOx/GCE as anode and Pt-PdNps/PGE as a cathode in oxygen-saturated 0.1 M PBS at pH 7.0 with different glucose concentrations. LSV was performed at 1.0 mVs^{-1} from the OCP of the cell to 0 V to evaluate the performance of the designed EBFCs. The current and power of the fuel cell were calculated using Ohm's Law ($V = I \times R$ and $P = I \times V$). The output density and current density were calculated from the apparent surface area of the anode. All the measurements were carried out at 37 °C.

The constructed glucose-based self-powered biofuel cell was tested using a sample of artificial blood serum containing 4.77 mM glucose. The performance of the designed EBFCs in real samples was also evaluated using LSV.

Results and Discussions

Characterization of Nanozyme-Based Cathode (Pt–Pd-Nps/PGE) and Its Electrochemical Response to ORR

In the first stage of the studies, the characterization of the cathode was carried out and its electrocatalytic activity with the reduction of O_2 was examined. It is well known that biocathodes consisting of enzymes such as bilirubin oxidase (BOx) and laccase (Lc) have been extensively used in developing EFCs due to their direct electron transfer ability and selectivity [23, 28–30]. These properties allow them to operate without a separation membrane to prevent cross-reactions at the electrodes [23]. Enzyme-mimicking nanomaterials called nanozymes have recently been introduced to biosensor and fuel cell studies [31–33]. In this study, PGEs modified with Pt–Pd bimetallic nanoparticles were used as nanozymes and have been proposed as a new cathode material in biofuel cell studies for the first time.

First, PtNps, PdNps, and Pt-PdNps were modified on PGE using electrochemical methods. SEM images, EDX spectra, and EDS mapping images were then recorded for unmodified and modified PGEs. SEM images (Fig. 1) show that the layered structures of unmodified PGE are homogeneously covered with nanoparticles obtained from monometal and bimetal deposition. Also, EDS mapping images were recorded for PGE, PtNps/PGE, PdNps/PGE, and Pt-PdNps/PGE electrodes and given Supplementary files (Fig. S1, Fig

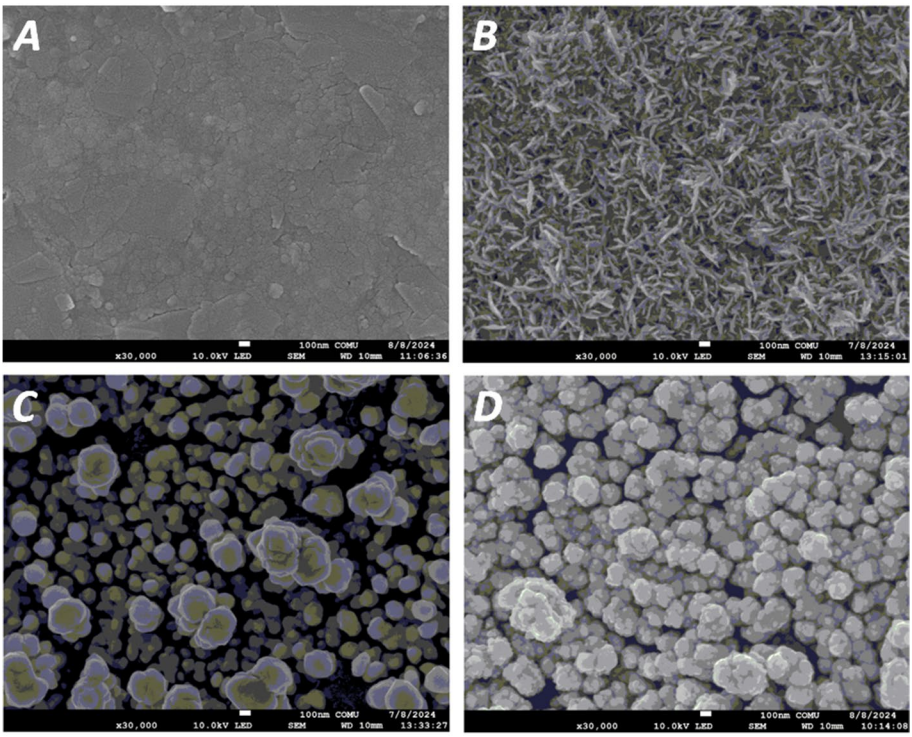

Fig. 1 SEM images of **A** unmodified PGE, **B** PtNps/PGE, **C** PdNps/PGE, and **D** Pt-PdNps/PGE electrodes

S2, Fig. S3 and Fig S4, respectively). According to EDX results (Fig. S6), it is expected to see 76.93% C, 17.68% O, 0.68% Mg, 1.53% Al, 0.25% Ca, 2% Fe, and 2.75% Si in unmodified PGE because pencil leads consist of clay and graphite [34]. In addition, 13.38% Pt in PtNps, 8.52% Pd in PdNps, and 4.27% Pt and 16.47% Pd in Pt-PdNps were found, which reflects that monometallic and bimetallic nanoparticles were successfully attached to the PGE surface.

EIS is widely used to understand electrode surface changes and resistance properties. The EIS curve consists of two main parts: the semicircle and the linear portion. These parts provide detailed information on the impedance changes of an electrode surface which is valuable for understanding modifications of electrode surfaces and their potential use in electrochemical sensing applications [35]. The linear portion of impedance spectra corresponds to the processes of electron transfer that are limited by diffusion. The semicircle is closely related to high frequencies and its diameter provides information about the charge transfer resistance (R_{ct}) which controls the electron transfer kinetics of the redox probe at the electrode's surface [35]. Thus, unmodified and modified PGEs were also electrochemically characterized by evaluating their CVs and EIS to understand electrode surface changes and surface resistance properties. EIS spectra of unmodified Pt-Nps/PGE, Pd-Nps/PGE, and PtPd-NPs/PGE were recorded in 5.0 mM $[Fe(CN)_6]^{3-/4-}$ containing 0.10 M KCl. The R_{ct} values obtained from Nyquist curves were obtained as 110, 37, 18, and 8 ohms for unmodified PGE, Pd-Nps/PGE, Pt-Nps/PGE, and PtPd-NPs/PGE, respectively (Fig. S7A). This is attributed to the fact that the metal nanoparticles speed up the transfer of electrons

on the surface of the PGE. CVs recorded in the redox probe for each electrode agree well with the EIS measurements. It can be seen from CVs that the highest peak currents of the redox probe were obtained from Pt-PdNps/PGE while the lowest peak currents were obtained from unmodified PGE (Fig. S7B).

To compare the electrocatalytic activities of the electrodes (bimetallic NPs-modified PGE), ORR was performed by using unmodified PGE and monometallic modified PGEs (PtNps/PGE and PdNps/PGE) together with Pt-PdNps/PGE as cathodes. Figure 2 shows the CVs and LSVs of these electrodes in the argon and oxygen-saturated 0.1 M KCl containing 0.1 M PBS at pH 7.0. It can be clearly seen that a remarkable enhancement in the electrocatalytic reduction of O_2 was observed at Pd-PtNps/PGE compared to unmodified PGE and the monometallic NPs-modified electrode. On the other hand, ORR has a high overpotential at unmodified PGE, and the current starting at 0 mV did not take the form of a peak but gradually increased by shifting potential in a more negative direction. ORR current of PtNps/PGE, PdNps/PGE, and Pt-PdNps/PGE were found to be 280, 340, and 570 µA at − 50, + 50, and + 90 mV vs. Ag/AgCl, respectively. It was concluded that Pt-PdNps/PGE is the most suitable electrode for the cathode in glucose/O_2 type EBFC because bimetallic nanoparticle-modified PGE has the highest peak current at a more positive voltage in the reduction potential compared to monometallic-modified PGEs.

Characterization and Electrochemical Behavior of Bioanode (MWCNT-Fc-GOx/GCE)

Direct electron transfer becomes difficult for GOx since the electroactive group is in the inner parts of the enzyme [3]. To overcome this situation, electrodes are modified with redox mediators such as ferrocene derivatives and osmium redox polymers [17, 19, 20]. In our previous studies, Ni nanoparticles and poly-pyrrole composites [36], nickel oxide-cobalt (II, III) oxide and nickel oxide-copper nanoparticles [37], and Cu nanoparticles [38] were used as redox mediators for nonenzymatic detection of glucose. Redox mediators facilitate electron transfer rates between substrate and electrode, resulting in an enhancement in electron transfer at the bioanode surface and in output power. In this study, ferrocene was immobilized with GOx onto MWCNT/GCE to obtain an effective bioanode.

To obtain the optimum MWCNT-Fc-GOx/GCE, which gives the most effective response to glucose oxidation, the GCE surface was optimized by adjusting the different

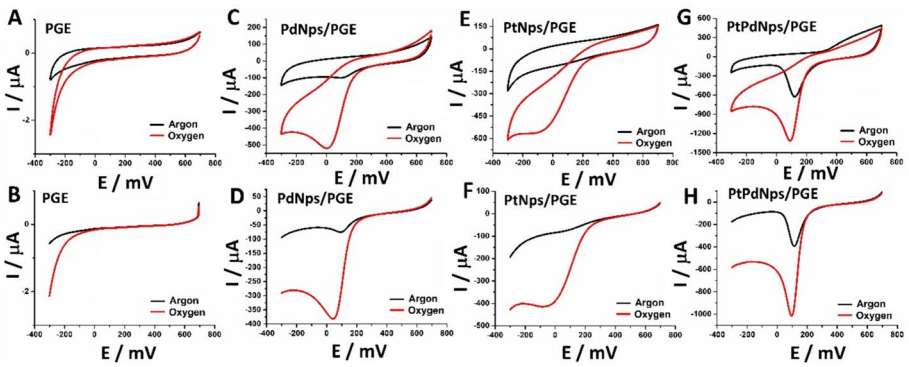

Fig. 2 CVs and LSVs of unmodified/PGE (**A** and **B**), Pd-Nps/PGE (**C** and **D**), Pt-Nps/PGE (**E** and **F**), and Pt–Pd-Nps/PGE (**G** and **H**) recorded in the supporting electrolyte with 0.1 M PBS at pH 7.0 saturated with argon (black) and oxygen (red) (scan rate: 25 mV/s)

concentrations of MWCNT, Fc, and GOx during the electrode preparation step. To determine the optimum electrode composition, CVs of each electrode prepared with different ratios of modification reagents were recorded in the absence and presence of 5.0 mM glucose. Figure S8. shows the curves of the concentration of modification reagents versus the electrocatalytic oxidation peak current of glucose. The maximum peak current for the electrocatalytic oxidation of glucose was achieved when MWCNT, Fc, and GOx (concentrations of 5.0 mg/mL, 25.0 mM, and 20.0 mg/mL, respectively) were immobilized onto the GCE surface.

The obtained optimum MWCNT-Fc-GOx/GCE was characterized by recording EIS and CVs in the 5.0 mM $Fe(CN)_6^{4-/3-}$ redox probe containing 0.10 M KCl. The Nyquist curves were used to estimate the R_{ct}, which was then used to evaluate the insulating properties of the electrode/electrolyte interface. Figure S9B shows that the R_{ct} values were found to be 1610 (Fig. S9B/c), 140 (Fig. S9B/b), and 580 (Fig. S9B/c) ohms for unmodified GCE, MWCNT-Fc-GCE, and MWCNT-Fc-GOx-GCE, respectively. R_{ct} value of unmodified GCE (1610 Ω) was remarkably decreased after the modification of both MWCNT and Fc (140 Ω) due to high surface area and conductivity of MWCNT and electrostatic interaction between positively charged Fc and negatively charged redox probe. These results indicate that the conductivity of the MWCNT-Fc/GCE which is directly related to its electron transfer ability is higher than that of the unmodified GCE. When the surface of MWCNT-Fc/GCE is immobilized with GOx, R_{ct} is increased to 580 ohms due to steric hindrance between the redox probe and large GOx. In addition, there is a good agreement between the CV results given in Fig. S9A and the EIS measurements given in Fig S9B. CVs from Fig S9A show that the highest peak currents of the redox probe were obtained from MWCNT-Fc/GCE, while the lowest peak currents were obtained from MWCNT-Fc-GOx/GCE. The information obtained from the voltammograms and impedance spectra indicates that MWCNT and Fc play an important role in increasing the electron transfer and conductivity properties between GCE and the $Fe(CN)_6^{3-/4-}$ redox probe. Finally, all these electroanalytical measurements indicate that the modification procedure with MWCNT-Fc and GOx was successful.

Additionally, the electrochemical CV data of the bioanode in the $Fe(CN)_6^{3-/4-}$ redox probe at different scan rates between 10 and 500 mVs^{-1} were used to determine the electrochemically active surface area. The Randles–Sevcik equation was used to determine the electroactive surface areas of the bare GCE, MWCNT-Fc/GCE, and MWCNT-Fc-GOx/GCE electrodes. According to this equation, $Ip = 2.69 \times 10^5 \times n^{3/2} \times A \times C_0 \times D^{1/2} \times v^{1/2}$, where Ip is the peak current (A), n is the number of the electrons, A is the electroactive surface area (cm^2), C_0 is the concentration of $Fe(CN)_6^{3-/4-}$ (5.0×10^{-6} mol cm^{-1}), and D is the diffusion coefficient for $Fe(CN)_6^{3-/4-}$ ($7.6 \times 10 - 6$ cm^2 s^{-1}) [39]. Electroactive surface areas of electrodes were calculated as 0.044 cm^2, 0.127 cm^2, and 0.088 cm^2 for GCE, MWCNT-Fc/GCE, and MWCNT-Fc-GOx/GCE, respectively. The high electroactive surface area of the MWCNT-Fc/GCE electrode is high due to the fast electron transfer rate of Fc between the electrode and electrolyte.

GOx is often used as a biocatalyst to produce biosensors and EBFCs. To evaluate the efficacy of MWCNT-Fc-GOx/GCE in catalyzing glucose oxidation, a series of comparative CVs were recorded in the absence and presence of glucose in a 0.1 M PBS with pH 7.0 containing 0.1 M KCl at a scan rate of 20 mVs^{-1}. It is expected that CV recorded by an unmodified GCE showed no anodic peaks attributed to glucose oxidation (Fig. 3A). Figure 3B(a) shows that the response of MWCNT-Fc-GOx/GCE in the absence of glucose. A well-defined redox couple with a formal potential of 300 mV indicates high activity and shows a characteristic, reversible redox peak behavior of Fc, in which a single electron transfer is involved for the

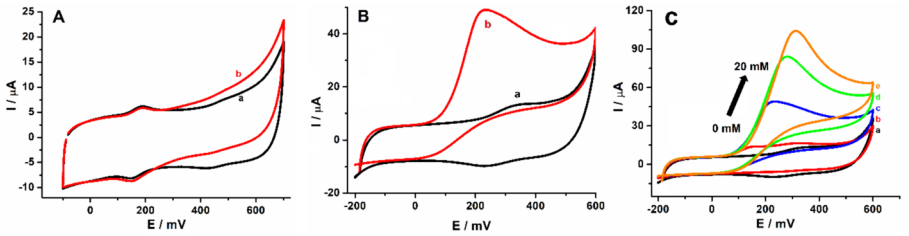

Fig. 3 CVs of **A** MWCNT-GOx/GCE and **B** MWCNT-Fc-GOx/GCE in the absence (a), presence (b) of 5.0 mM glucose, and **C** MWCNT-Fc-GOx/GCE electrode in different glucose concentrations in 0.1 M pH 7.0 PBS containing 0.1 M KCl at a scan rate of 20 mV/s

electro-oxidation peak current of Fc. Also, electrocatalytic oxidation of glucose was observed at the GOx immobilized on the MWCNT-Fc/GCE surface (Fig. 3B(b)). The anodic peak of the MWCNT-Fc-GOx/GCE remarkably increased in the presence of 10 mM of glucose, while in the presence of the same glucose concentration, the cathodic peaks slightly decreased (Fig. 3B(b)). Therefore, the significant increase in the anodic peak of the modified electrodes when exposed to glucose demonstrates the excellent oxidative electrocatalytic activity of the GOx with electrocatalyst (Fc) towards glucose. Considering that the GCE area, which is 0.07 cm^2, results in a high current density, fast charge transfer on the GCE proves its suitability for electrode modification with GOx, Fc, and MWCNT. CVs of MWCNT-Fc-GOx/GCE were also measured at different glucose concentrations ranging from 0 to 20 mM (Fig. 3C). The electrodes exhibited a higher oxidative current response with increasing glucose concentrations. They showed the same onset potential (approximately − 0.1 V vs. Ag/Ag^+) in the CV test, which is dependent on the activation of the glucose oxidation reaction. The successful immobilization of enzymes on the electrode surface and electron transfer between the enzyme and electrode via Fc mediator is also successfully achieved with Fc-MWCNTs modified electrodes.

In the GOx-catalyzed oxidation of glucose, FAD is reduced to $FADH_2$ and subsequently re-oxidized by O_2:

$$\boldsymbol{\beta - D - glucose + FAD - GOx \rightarrow D - gluconolactone + FADH_2 - GOx}$$

$$\boldsymbol{FADH_2 - GOx + O_2 \rightarrow FAD - GOx + H_2O_2}$$

Oxygen can be replaced by redox reagents, including ferrocene derivatives. Additionally, ferrocene/ferricinium (Fc/Fc^+) couples have been employed for heterogeneous mediation of electron transfer between GOx and amperometric electrodes [40]. Given that FAD is situated at a depth of > 13 A° below the surface of GOx, direct electron transfer between the enzyme and an electrode surface is not observed [40]. However, free FAD is capable of transferring electrons with a variety of electrodes, as outlined in the following equation:

$$\boldsymbol{FAD + 2H^+ + 2e^- \leftrightarrow FADH_2}$$

In our scheme, a glucose-sensitive electrocatalytic current results from the oxidation of Fc at the electrode surface and its reduction by $FADH_2$ by intramolecular electron transfer:

$$\boldsymbol{FADH_2 - GOx - (Fc)_n \leftrightarrow FADH_2 - GOx - (Fc^+)_n + ne^-}$$

$$FADH_2 - GOx - (Fc^+)_n \rightarrow FAD - GOx - (Fc)_2(Fc^+)_{n-2} + 2H^+$$

The electrocatalytic glucose oxidation at the enzymatic electrode (MWCNT-Fc-GOx/GCE) was also investigated by chronoamperometry (CA). To assess the effect of applied potential on the response to glucose, CAs were recorded for MWCNT-Fc-GOx/GCE at various potentials ranging from 0.20 to 0.5 V. This was achieved by adding 1 mM glucose successively into a continuously stirred 10 mL solution of 0.10 M pH 7.0 PBS containing 0.1 M KCl. The results show that the maximum peak current was obtained when the applied potential was fixed at 0.30 V vs Ag/AgCl. CAs of MWCNT-GOx/GCE and MWCNT-Fc-GOx/GCE at 0.30 V were recorded based on the successive addition of glucose in the range from 1 to 10 mM. The CAs in Fig. 4A were recorded within approximately 5 s of adding glucose and indicate a steady-state current. Additionally, it can be observed that these steady-state currents increased as the glucose concentration increased. The MWCNT-GOx/GCE (as shown in Fig. 4A, red line) does not respond to glucose. However, the MWCNT-Fc-GOx/GCE electrode responds well to glucose. The signal

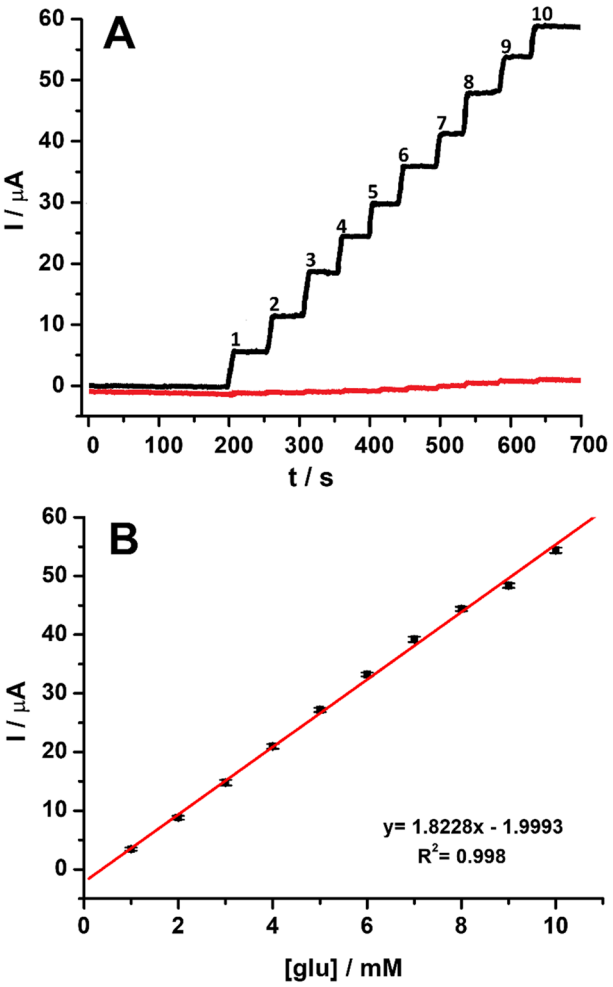

Fig. 4 Chronoamperomograms of **A** MWCNT-GOx/GCE and MWCNT-Fc-GOx/GCE (black line) recorded by the successive addition of 1.0 mM glucose into continuously stirred (at 100 rpm) 10 mL supporting electrolyte (0.10 M of PBS at pH 7.0) at E_{bias} of 0.30 V registered at 0.30 V. **B** Calibration plot obtained from chronoamperomogram of glucose recorded for MWCNT-Fc-GOx/GCE

recorded by the modified GCE (Fig. 4, black line) was higher than that of the MWCNT-GOx/GCE. The calibration plot suggests a linear relationship between current and glucose concentration, which varied from 1 to 10 mM during the study of MWCNT-Fc-GOx/GCE (Fig. 4B). To calculate the limit of detection (LOD), the limit of quantification (LOQ), and sensitivity values of the proposed sensor, the lowest concentration that gives an amperometric response was recorded ten times. The LOD and LOQ were calculated according to the equation of $3 \times SD/m$ and $10 \times SD/m$ ("SD," the standard deviation for peak currents; and "m," the slope calculated from the calibration curve) and determined as 0.26 mM and 0.87 mM, respectively. Also the sensitivity of the proposed sensor was calculated 25.71 μ A/mM.

During the final step of anode characterization, the influence of potentially interfering compounds, such as other monosaccharides (galactose, mannose, fructose, maltose), disaccharides (sucrose), uric acid (UA), dopamine (DA), and ascorbic acid (AA), on the response to glucose was examined at MWCNT-Fc-GOx/GCE. For this purpose, the steady-state background current was stabilized under the optimized conditions. The CAs of MWCNT-Fc-GOx/GCE were recorded by adding known volumes of stock solutions of glucose and interfering compounds to an electrochemical cell. The concentrations of glucose and each interfering compound were fixed at the same concentration. Table S1 demonstrates the response of interference molecules toward glucose. The results show that the designed anode electrode was minimally affected by fructose, sucrose, maltose, mannose, galactose, glutamic acid, lactose, and sodium lactate while highly affected by UA, AA, and DA. It is well known that these substances exhibit positive interference effects by oxidizing at high anodic potentials and enhancing the glucose biosensor's signal. Our previous studies showed that a pre-oxidant ($NaBiO_3$) was successfully used to minimize the interference of these substances [41]. Thus, solutions, including glucose and interference substances, were passed from $NaBiO_3$ filled in an injector several times. After that, the interference effects of UA, DA, and AA were significantly reduced by their pre-oxidation with $NaBiO_3$, while glucose was not oxidized by $NaBiO_3$. The results indicate that MWCNT-Fc-GOx/GCE demonstrates a high selectivity towards glucose.

Fuel Cell Performance and Real Sample Analysis

Glucose was chosen as a biofuel model in our BFC development because it is one of the significant components of human biofluids including blood, tears, saliva, and sweat. The fuel cell performance of the system was evaluated by monitoring power output and current density dependent on OCP in air-saturated PBS containing 0.10 M KCl and various concentrations of glucose in the range from 1 to 10 mM. The maximum current density of 460 $\mu A/cm^2$ and a maximum power output of 32.05 $\mu W/cm^2$ were obtained at a voltage of 0.285 V (Fig. 5). The high current and power density were achieved due to the customized composite electrodes in both the anode and cathode. These electrodes possess desirable electrical conductivity and electrocatalytic properties. The hybrid MWCNT-Fc enables an efficient transfer of electrons from the anode to the cathode, significantly increasing the power output. Figure 5B demonstrates a positive correlation between glucose concentration and power density within the 0–10 mM glucose range. The response generated by the BFC was observed with successive additions of glucose in the range of 0–10 mM. The calibration plot for the self-generated current signal demonstrates linearity up to 10 mM glucose. This observation provides strong evidence for the ability of the BFC to detect glucose levels in this range.

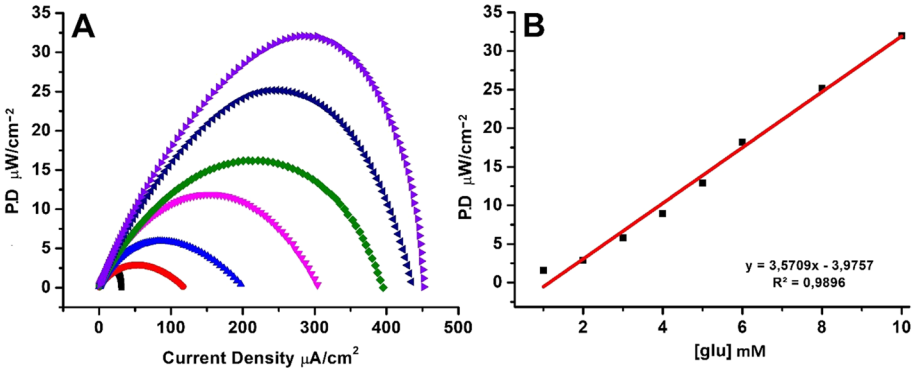

Fig. 5 **A** Power and current density curves at various concentrations with designed EBFC with the anode (MWCNT-Fc-GOx/GCE) and the cathode (Pt–Pd-Nps/PGE). **B** Calibration plot obtained from power density values

Table 1 compares the performance of the designed glucose-based EBFC with the previously reported EBFCs. As can be seen from Table 1, the proposed glucose-based EBFC demonstrates better performance than some other previously reported EBFCs in terms of power density values. Furthermore, the designed electrode for the cathode has never been used previously for ORR. PGEs have several benefits, including disposability, affordability, mechanical rigidity, simplicity, commercial availability, and ease of surface modification [42]. Also, nanozymes have many advantages such as diverse enzyme-mimicking activities, low cost, high stability, robustness, unique surface chemistry, ease of surface tunability, and biocompatibility. Therefore, our cathode design brings the advantages of PGE and nanozymes together. The mechanism of Pt–Pd-Nps/PGE boosting the electrochemical reduction of oxygen can be attributed to the synergistic effect of Pt and Pd nanoparticles which makes oxygen reduction at the cathode surface more efficient. Additionally, the cathode electrode can reduce oxygen to water without the need for enzymes such as BOx and Lc.

The investigation was also conducted to determine the performance of the designed EBFC with artificial serum samples. To attain the desired outcome, the glucose levels in artificial serum samples were measured by the LSV method, and the voltammograms for each sample were recorded under optimized conditions. At 0.280 V, a maximum current density of 290 $\mu A/cm^2$ and a maximum power output of 11.35 $\mu W/cm^2$ were achieved using 10 mM glucose (Fig. S10). This study has shown that designed EBFC can be effectively used for glucose determination in real and artificial samples and suggests their potential as simple to configure energy-sustaining and noninvasive glucose monitoring devices.

Conclusion

Combining bimetallic and enzymatic catalysts has been suggested as a unique approach to moderate-condition glucose oxidation. This study presents the first evaluation of PGE modified with Pt–Pd bimetallic nanoparticles for oxygen reduction at the cathode. Furthermore, the membraneless design of our EBFC presents another advantage for the developed system. When glucose concentration is 10 mM or higher, the EBFC exceeds a maximal registered open-circuit voltage of 0.285 V. The maximal power density was

Table 1 Comparison of the analytical performance of proposed self-powered EBFC with some previously reported EBFCs in the literature

BFC/analyte	Anode	Cathode	OCP (mV)	Power density (mW/cm^2)	Current density (mA/cm^2)	Reference
Glucose/O_2	GDH/poly(TBO)/GCE	GOx/HRP/MWCNT/GE	650.0	31.3	165.9	[43]
Glucose/O_2	GRE/5AP/GOx	GRE/HRP/GOx	450.0	3.5	22.0	[44]
Glucose/O_2	PGE/MWCNT/GOx	PGE/MWCNT/laccase	433.0	18.0	60.0	[45]
Glucose/O_2	PPD/(AuNPs)PPCA−GOx	GRE/PB-PPCA/PPCA−GOx	640.0	10.94	60.52	[5]
Glucose/O_2	GDH-MB	GOx-hemin	500.0	18.0	230.0	[46]
Glucose/O_2	PPy–GOD–CNT	PPy–CNT–laccase	-	37.4	-	[47]
Glucose/O_2	MWCNT-PCA/Ca^{2+}/GOx	rGC	140.0	6.25	-	[48]
Glucose/O_2	Fc-Go/GCE	BOx-$ABTS^{2-}$/fBP	200.0	26	-	[49]
Glucose/O_2	***MWCNT-Fc-GOx/GCE***	***PtPd-Nps/PGE***	***285.0***	***32.05***	***460.0***	***This work***

rGC reduced graphene oxide-ceria, *MWCNT-PCA* multiwalled carbon nanotube-pyrene carboxylic acid, *Fc* ferrocene, *GCE* glassy carbon electrode, *ABTS* 2,2′-azinobis(3-ethylbenzothiazoline-6-sulfonate) diammonium salt, *fBP* functionalized bucky paper, *Pt–Pd-Nps* Pt–Pd nanoparticles, *PPy* poly-pyrrole, *BOx* bilirubin oxidase, *GDH* glucose dehydrogenase, *MB* methylene blue, *PPD* poly(1,10-phenanthroline-5,6-dione), *PB* Prussian blue, *PPCA* poly(pyrrole-2-carboxylic acid), *MWCNT* multi-walled carbon nanotube, *HRP* horseradish peroxidase

calculated to be 32.05 μW/cm^2 when the cell voltage was 0.285 V and glucose was 10 mM. This could be attributed to the enhanced energetic efficiency due to the use of Fc serving as a mediator for GOx and Pt–Pd bimetallic Nps for ORR. Also, MWCNT can significantly enhance the efficacy of EBFCs by increasing the effective electrode area. In conclusion, the novel EBFC design proposed in this study is a promising candidate for detecting glucose in natural and artificial fluids. The obtained results also indicate the potential use of the designed EBFC in energy sustaining and noninvasive glucose monitoring devices.

Supplementary Information The online version contains supplementary material available at https://doi.org/10.1007/s12010-024-05068-1.

Author Contribution Gamze Emir: investigation, methodology, analysis, and writing original draft; Samet Şahin: editing, conceptualization, review, and supervision; Yusuf Dilgin: editing, review, and supervision; Cahit Akgül: writing, review and editing, conceptualization, and supervision.

Funding We appreciate the Scientific Research Projects Coordination Unit of Çanakkale Onsekiz Mart University (FDK-2022–4073) for financial support. This study was produced as a part of the PhD thesis of Gamze Emir GUNAY.

Data Availability The data that support the findings of this study are not openly available and are available from the corresponding author upon reasonable request.

Declarations

Ethical Approval Not applicable.

Consent to Participate Not applicable.

Consent for Publication We declare that the information in this manuscript has not been published elsewhere nor is it under consideration by any other journal. Furthermore, it is the consensus of all authors to submit this manuscript for possible publication in ABB.

Competing Interests The authors declare no competing interests.

References

1. Barelli, L., Bidini, G., Pelosi, D., & Sisani, E. (2021). *Energies, 14*(4), 910.
2. Chengcheng, G., Gai, P., & Li, F. (2022). *Nano Energy, 93*, 106806.
3. Sahin S, T. Wongnate, L. Chuaboon, P. Chaiyen, E.H. Yu, 2018 Biosensors and Bioelectronics 107 17-25
4. X. Xiao, H.Q. Xia, R. Wu, L. Bai, L. Yan, E. Magner, S. Cosnier, E. Lojou, Z. Zhu, A. Liu, 2019 Chem Rev 28 119(16) 9509–9558
5. Kausaite-Minkstimiene, A., Kaminskas, A., & Ramanaviciene, A. (2022). *Biosensors & Bioelectronics, 216*, 114657.
6. Nasar, A., & Perveen, R. (2019). *International Journal of Hydrogen Energy, 44*(29), 15287–15312.
7. Gu, C., Gai, P., & Li, F. (2022). *Nano Energy, 93*, 106806.
8. Li, Z., Kang, Z., & Zhu, Z. (2022). *Journal of Chemical Engineering, 428*, 131258.
9. K. Veenuttranon, K. Kaewpradub, I. Jeerapan, 2023 Nano-Micro Letters 15(85)
10. Jeerapan, I., Sangsudcha, W., & Phokhonwong, P. (2022). *Sensing Biosensing Researsch, 38*, 100525.
11. Rasmussen, M., Abdellaoui, S., & Minteer, S. D. (2016). *Biosensors & Bioelectronics, 76*(15), 91–102.
12. Harkness, J. K., Murphy, O. J., & Hitchens, G. D. (1993). *Journal of Electroanalytical Chemistry, 1–2*, 261–272.
13. Huang, W., Zulkifli, M. Y. B., Chai, M., Lin, R., Wang, J., Chen, Y., Chen, V., & Hou, J. (2023). *Journal Science Exploration, 3*(4), 20220145.

14. Liang, J., Huang, Q., Wu, L., Shi, X., Yan, K., Guo, F., Zhou, Z., & Li, G. (2024). *Microchemical Journal, 200*, 110478.
15. Yu, J., Chen, T., Wen, X., Shi, H., Wang, L., & Xu, Y. (2024). *Biosensors & Bioelectronics, 253*, 116169.
16. Teoman, I., Karakaya, S., & Dilgin, Y. (2019). *Analytical Letters, 52*(13), 2041–2056.
17. J. Wang, 2004 Electroanal 7–14
18. Jin, X., Li, G., Xu, T., Su, L., Yan, D., & Zhang, X. (2021). *Electroanal, 33*, 1902–1910.
19. G.R. WandeZande, J.M. Olvany, J.L. Rutherford, M. Rasmussen, 2016 Enzyme Stabilization and Immobilization 165–179
20. Wang, Y., Wang, Q., Chai, G., Fan, W., Shi, Q., Zhang, W., Mao, J., Xie, J., Wei, R., & Zhang, Q. (2023). A flexible electrochemical glucose sensing platform based on an electrospun PVA mat covered with in situ grown silver nanoparticles and a mixed self-assembled monolayer of glucose oxidase and ferrocene. *The Analyst, 148*, 3724–3729.
21. Hoshi, N., Nakamura, M., Kubo, R., & Suzuki, R. (2024). Enhanced oxygen reduction reaction on caffeine-modified platinum single-crystal electrodes. *Communications Chemistry, 7*, 23.
22. B. Das, J.L. Franco, N. Logan, P. Balasubramanian, M.I. Kim, C. Cao, Nano-Micro Commun., 2021, 13(193)
23. Mano, N., & de Poulpiquet, A. (2018). *Chemical Reviews, 118*, 2392–2468.
24. Jiang, D., Ni, D., Rosenkrans, Z., Huang, P., Yan, X., & Cai, W. (2019). *Chemical Society Reviews, 48*(14), 3683–3704.
25. Wu, J., Wang, X., Wang, Q., Lou, Z., Li, S., Zhu, Y., Qin, L., & Wei, H. (2019). *Chemical Society Reviews, 48*, 1004–1076.
26. Karakaya, S., & Dilgin, Y. (2017). Flow injection amperometric analysis of H2O2 at platinum nanoparticles modified pencil graphite electrode. *Electroanalysis, 29*(6), 1626–1634.
27. Karakaya, S., & Dilgin, Y. (2019). Sensitive flow-injection electrochemical determination of hydrogen peroxide at a palladium nanoparticle-modified pencil graphite electrode. *Analytical Letters, 52*(6), 998–1017.
28. Wang, L., Wu, X., Qi-wen Su, B. S., Song, R., Zhang, J.-R., & Zhu, J.-J. (2021). Enzymatic biofuel cell: Opportunities and intrinsic challenges in futuristic applications. *Advanced Energy and Sustainability Research, 2*, 2100031.
29. Torrigino, F., Nagel, M., Peng, Z., Hartmann, M., & Herkendell, K. (2023). *Catalysts, 13*, 1415.
30. M. Munjal, D.K. Yadav, R.K. Sharma, G. Singh, 2021 Biofuel Cells, Materials and Challenges 12
31. Romanholo, P. V. V., Razzino, C. A., Raymundo-Pereira, P. A., Prado, T. M., Machado, S. A. S., & Sgobbi, L. F. (2021). *Biosensors & Bioelectronics, 185*, 113242.
32. Das, B., Franco, J. L., Logan, N., Balasubramanian, P., Kim, M. I., & Cao, C. (2021). *Nano-Micro Lett., 19*, 193.
33. Jiang, D., Ni, D., Rosenkrans, Z. T., Huang, P., Yan, X., & Cai, W. (2019). *Chemical Society Reviews, 48*, 36.
34. Annu, S., Sharma, R., & Jain, A. N. R. (2020). *Journal of the Electrochemical Society, 167*, 037501.
35. Suni, I. I. (2008). *TrAC, Trends in Analytical Chemistry, 27*(7), 604–611.
36. Emir, G., Dilgin, Y., Ramanaviciene, A., & Ramanavicius, A. (2021). *Microchemical Journal, 161*, 105751.
37. Ayaz, S., Karakaya, S., Emir, G., Dilgin, D. G., & Dilgin, Y. (2022). *Analytical Letters, 55*(13), 2046–2057.
38. Ayaz, S., Karakaya, S., Emir, G., Dilgin, D. G., & Dilgin, Y. (2020). *Microchemical Journal, 154*, 104586.
39. Ersan, T., Dilgin, D. G., Kumrulu, E., Kumrulu, U., & Dilgin, Y. (2023). *Electroanalysis, 35*(4), 202200295.
40. Badia, A., Carlini, R., Fernandez, A., Battaglini, F., Mikkelsen, S. R., & English, A. M. (1993). *Journal of the American Chemical Society, 115*(16), 1394.
41. Gunes, M., Karakaya, S., & Dilgin, Y. (2020). *Chemical Papers, 74*, 1923–1936.
42. Dilgin, D. G., Vural, K., Karakaya, S., & Dilgin, Y. (2024). *Monatshefte fuer Chemie, 155*, 143–153.
43. K. Chansaenpak, A. Kamkaew, S. Lisnund, P. Prachai, P. Ratwirunkit, T. Jingpho, V. Blayi P. Pinyou, 2021 Biosensors 11(1), 16
44. V. Krikstolaityte, Y. Oztekin, J. Kuliesius, A. Ramanaviciene, Z. Yazıcıgil, M. Ersoz, A. Okumus, A. Kausaite-Minkstimiene, z. Kilic, A. O. Solak, A. Makaraviciute, A. Ramanavicius, 2013 Electroanalysis 25(12), 2677–2683
45. Rewatkar, P., Bandapati, M., & Goel, S. (2019). *International Journal of Hydrogen Energy, 44*(59), 31434–31444.
46. A. Koushanpour, M. Gamella, N. Guzi E. Katz, 2017 Electroanalysis 29, 950–954
47. Kim, J., & Yoo, K. H. (2013). *Physical Chemistry Chemical Physics: PCCP, 15*, 3510–3517.

48. Arjun, A. M., Vimal, M., & Sandhyarani, N. (2019). *International Journal of Hydrogen Energy, 44*(49), 27056–27066.
49. Bunte, C., Hussein, L., & Urban, G. A. (2014). *Journal of Power Sources, 247*, 579–586.

Authors and Affiliations

Gamze Emir[1] · Yusuf Dilgin[1] · Samet Şahin[2,3] · Cahit Akgul[1]

✉ Gamze Emir
gamze.emir@comu.edu.tr

✉ Cahit Akgul
cahitakgul@comu.edu.tr

[1] Chemistry Department, Faculty of Science, Canakkale Onsekiz Mart University, Canakkale, Turkey

[2] School of Engineering, Lancaster University, Lancaster LA1 4YW, UK

[3] Bioengineering Department, Faculty of Engineering, Bilecik Seyh Edebali University, Bilecik, Turkey